Astron. Astrophys. 363, 425–439 (2000)

ASTRONOMY AND ASTROPHYSICS

Equilibrium configurations of perfect fluid orbiting Schwarzschild–de Sitter black holes

Z. Stuchlík, P. Slaný⋆, and S. Hledík

Silesian University, Department of Physics, Faculty of Philosophy and Science, Bezručovo nám. 13, Opava, Czech Republic (zdenek.stuchlik@fpf.slu.cz; petr.slany@vsb.cz; stanislav.hledik@fpf.slu.cz)

Received 30 May 2000 / Accepted 15 September 2000

Abstract. The hydrodynamical structure of perfect fluid orbiting Schwarzschild–de Sitter black holes is investigated for configurations with uniform distribution of angular momentum density. It is shown that in the black-hole backgrounds admitting the existence of stable circular geodesics, closed equipotential surfaces with a cusp, allowing the existence of toroidal accretion disks, can exist. Two surfaces with a cusp exist for the angular momentum density smaller than the one corresponding to marginally bound circular geodesics; the equipotential surface corresponding to the marginally bound circular orbit has just two cusps. The outer cusp is located nearby the static radius where the gravitational attraction is compensated by the cosmological repulsion. Therefore, due to the presence of a repulsive cosmological constant, the outflow from thick accretion disks can be driven by the same mechanism as the accretion onto the black hole. Moreover, properties of open equipotential surfaces in vicinity of the axis of rotation suggest a strong collimation effects of the repulsive cosmological constant acting on jets produced by the accretion disks.

Key words: accretion, accretion disks – black hole physics – gravitation – relativity – galaxies: quasars: general

1. Introduction

Recent observations give strong evidence that the energy sources of quasars and active galactic nuclei are accretion disks around central massive black holes (Abramowicz & Percival 1997; Blandford 1990). Similar, scaled down, accretion disks appear in some extraordinary galactic binary systems containing a black hole (or a neutron star). In the accretion disks, the potential gravitational energy of matter orbiting the central black hole is liberated and transferred into heat, due to viscous stresses acting against shearing motion, and radiated (at least partly) away. During the process, angular momentum of the accreting matter has to be transported outwards.

It is well known that at low accretion rates the pressure is negligible, and the accretion disk is geometrically thin. Its basic properties are determined by the circular geodesic motion in the black-hole background. The radius $r_{\rm ms}$ of the marginally stable circular orbit represents the inner edge of the Keplerian disks, since matter, following quasikeplerian orbits down to $r_{\rm ms}$, falls freely into the black hole from this radius (Novikov & Thorne 1973; Stoeger 1976). At high accretion rates, the pressure is relevant, and the accretion disk must be geometrically thick. Its basic properties are determined by equipotential surfaces of test perfect fluid (i.e., perfect fluid that does not alter the black-hole geometry) rotating in the black-hole background. The accretion is possible, if a toroidal equilibrium configuration of the test fluid containing a critical, self-crossing equipotential surface can exist in the background. The cusp of this equipotential surface corresponds to the inner edge of the disk, and the accretion inflow of matter into the black hole is possible due to a mechanical non-equilibrium process, i.e., because of matter slightly overcoming the critical equipotential surface. The pressure gradients push the inner edge of the thick disks under the radius $r_{\rm ms}$ (Kozlowski et al. 1978; Abramowicz et al. 1978).

The simplest, but quite illustrative case of the equipotential surfaces of the test fluid can be constructed for the configurations with uniform distribution of the angular momentum density. This case is fully governed by the geometry of the spacetime, however, it contains all the characteristic features of more complex cases of the rotation of the fluid (Jaroszyński et al. 1980). Moreover, this case is also very important physically since it corresponds to marginally stable equilibrium configurations (Seguin 1975).

The equipotential surfaces were analyzed for both Schwarzschild and Kerr black-hole spacetimes. The critical closed surfaces with a cusp can exist for angular momentum density higher (lower) than the one corresponding to the marginally stable (bound) circular geodesic, and the location of the cusp shifts from $r_{\rm ms}$ to the radius of the marginally bound geodesic orbit $r_{\rm mb}$. The cusp close to the horizon enables the inflow of matter into the black hole. However, the character of the equilibrium configurations does not allow outflow of matter and transfer of the angular momentum for disks around isolated black holes. In binary systems the outflow is possible through the Lagrange point L2 – see, e.g., Novikov & Thorne (1973).

Very recently, a wide variety of cosmological observations (measurements of the present value of the Hubble parameter, de-

Send offprint requests to: Z. Stuchlík

⋆ *Present address:* Technical University at Ostrava, Department of Physics, Faculty of Mining, Ostrava, Czech Republic

tails of the anisotropy of the cosmic relic radiation, statistics of gravitational lensing of quasars, and high-redshift supernovae) suggest a non-zero, repulsive cosmological constant (Krauss & Turner 1995; Ostriker & Steinhardt 1995; Krauss 1998). Therefore, it is interesting to clarify the influence of the repulsive cosmological constant on astrophysically relevant properties of black-hole spacetimes.

Here, we shall show that in the field of black-hole spacetimes with a repulsive cosmological constant the outflow of matter from the accretion disk is possible, because equipotential surfaces with an outer cusp in vicinity of the so called static radius can exist (beside the critical surfaces with the inner cusp nearby the horizon), if the mass of the black hole is small enough to admit existence of the stable circular geodesics (Stuchlík & Hledík 1999). Moreover, if the uniform angular momentum density of the equilibrium configuration corresponds to the marginally bound orbit of the background, the critical equipotential surface has both the inner and outer cusps. In this situation, any mechanical non-equilibrium in the thick disk leads to both inflow into the black hole, and outflow from the disk near the static radius.

The plan of this paper is following. In Sect. 2, the basic formulae for the equilibrium configurations of test perfect fluid in a given stationary and axially symmetric background are summarized, following the papers of Abramowicz and coworkers (Kozlowski et al. 1978; Abramowicz et al. 1978; Jaroszyński et al. 1980). In Sect. 3, the equipotential surfaces of the marginally stable configurations (having a uniform distribution of angular momentum density) of the test perfect fluid are determined for the Schwarzschild–de Sitter black-hole spacetimes. For completeness, we include also discussion of the case of the Schwarzschild–anti-de Sitter spacetimes with an attractive cosmological constant. In Sect. 4, some concluding remarks are presented, and astrophysical consequences of the presented results are pointed out. We shall use the geometric system of units ($c = G = 1$), if not stated otherwise.

2. Boyer's condition for equilibrium configurations of test perfect fluid

We briefly summarize the well known results of a general theory of the equipotential surfaces inside any relativistic, differentially rotating, perfect fluid body (Boyer 1965; Abramowicz 1974), applied to test configurations of perfect fluid rotating in the stationary and axially symmetric spacetimes (Kozlowski et al. 1978; Abramowicz et al. 1978; Jaroszyński et al. 1980). In the standard coordinate system the spacetimes are described by the line element

$$\mathrm{d}s^2 = g_{tt}\,\mathrm{d}t^2 + 2g_{t\phi}\,\mathrm{d}t\mathrm{d}\phi + g_{\phi\phi}\,\mathrm{d}\phi^2 + g_{rr}\,\mathrm{d}r^2 + g_{\theta\theta}\,\mathrm{d}\theta^2, \quad (1)$$

where the metric coefficients depend neither on the time coordinate, t, nor the azimuthal coordinate, ϕ, i.e., the spacetimes contain timelike and azimuthal Killing vector fields $\partial/\partial t$ and $\partial/\partial\phi$.

We shall consider test perfect fluid rotating in the ϕ direction. Its four velocity vector field U^μ has, therefore, only two non-zero components

$$U^\mu = (U^t, U^\phi, 0, 0), \quad (2)$$

which can be functions of the coordinates r, θ. The stress-energy tensor of the perfect fluid is

$$T^\mu{}_\nu = (p + \epsilon)U^\mu U_\nu + p\,\delta^\mu_\nu, \quad (3)$$

where ϵ and p denote the total energy density and the pressure of the fluid. The rotating fluid can be characterized by the vector fields of the angular velocity Ω, and the angular momentum per unit mass (angular momentum density) ℓ, defined by

$$\Omega = \frac{U^\phi}{U^t}, \quad \ell = -\frac{U_\phi}{U_t}. \quad (4)$$

These vector fields are related by

$$\Omega = -\frac{g_{t\phi} + \ell g_{tt}}{g_{\phi\phi} + \ell g_{t\phi}}. \quad (5)$$

In static spacetimes ($g_{t\phi} = 0$), the relation (5) reduces to a simple formula

$$\frac{\Omega}{\ell} = -\frac{g_{tt}}{g_{\phi\phi}}. \quad (6)$$

The surfaces of constant ℓ and Ω are called von Zeipel's cylinders. The family of von Zeipel's cylinders does not depend on the assumed rotation law of the fluid, $\ell = \ell(\Omega)$, in the static spacetimes, but it will depend on the rotation law in the stationary spacetimes (with $g_{t\phi} \neq 0$) (Kozlowski et al. 1978).

Projecting the energy conservation law $T^{\mu\nu}{}_{;\nu} = 0$ onto the hypersurface orthogonal to the four velocity U^μ by the projection tensor $h_{\mu\nu} = g_{\mu\nu} + U_\mu U_\nu$, we obtain the relativistic Euler equation in the form

$$\frac{\partial_\mu p}{p + \epsilon} = -\partial_\mu(\ln U_t) + \frac{\Omega\,\partial_\mu \ell}{1 - \Omega\ell}, \quad (7)$$

where

$$(U_t)^2 = \frac{g_{t\phi}^2 - g_{tt}\,g_{\phi\phi}}{g_{\phi\phi} + 2\ell g_{t\phi} + \ell^2 g_{tt}}. \quad (8)$$

The solution of the relativistic Euler equation can be given by Boyer's condition determining the surfaces of constant pressure through the "equipotential surfaces" of the potential $W(r, \theta)$ by the relations (Abramowicz et al. 1978)

$$\int_0^p \frac{\mathrm{d}p}{p + \epsilon} = W_{\mathrm{in}} - W, \quad (9)$$

$$W_{\mathrm{in}} - W = \ln(U_t)_{\mathrm{in}} - \ln(U_t) + \int_{\ell_{\mathrm{in}}}^{\ell} \frac{\Omega\,\mathrm{d}\ell}{1 - \Omega\ell}; \quad (10)$$

the subscript "in" refers to the inner edge of the disk. For an alternative definition of Boyer's condition see (Abramowicz et al. 1978; Fishbone & Moncrief 1976; Fishbone 1977). The equipotential surfaces are determined by the condition

$$W(r, \theta) = \mathrm{const}, \quad (11)$$

and in a given spacetime can be found from Eq. (10), if a rotation law $\Omega = \Omega(\ell)$ is given. The surfaces of constant pressure $p(r,\theta) = \mathrm{const}$ are given by Eq. (9). The structure of thick accretion disks can be obtained also in the framework of a very practical and accurate Newtonian model for the gravitational field of a non-rotating black hole, known as the Paczyński–Wiita potential (Paczyński & Wiita 1980; Abramowicz et al. 1980).

3. Equipotential surfaces of the marginally stable configurations orbiting Schwarzschild–de Sitter black holes

Equilibrium configurations of test perfect fluid rotating around an axis of rotation in a given spacetime are determined by the equipotential surfaces, where the gravitational and inertial forces are just compensated by the pressure gradient. (In an axially symmetric spacetime, the axis of rotation coincides with the axis of symmetry of the spacetime, while in a spherically symmetric spacetime the axis of rotation can be any radial line; usually, the coordinate system is chosen so that the rotation axis corresponds to $\theta = 0$.)

The equipotential surfaces can be closed or open. Moreover, there is a special class of critical, self-crossing surfaces (with a cusp), which can be either closed or open. The closed equipotential surfaces determine stationary equilibrium configurations. The fluid can fill any closed surface—at the surface of the equilibrium configuration pressure vanish, but its gradient is non-zero (Kozlowski et al. 1978). On the other hand, the open equipotential surfaces are important in dynamical situations, e.g., in modeling jets (Lynden-Bell 1969; Blandford 1987). The critical, self-crossing closed equipotential surfaces W_{cusp} are important in the theory of thick accretion disks, because accretion onto the black hole through the cusp of the equipotential surface located in the equatorial plane is possible due to the Paczyński mechanism.

According to Paczyński, the accretion into the black hole is driven through the vicinity of the cusp due to a little overcoming of the critical equipotential surface, $W = W_{\mathrm{cusp}}$, by the surface of the disk. The accretion is thus driven by a violation of the hydrostatic equilibrium, rather than by viscosity of the accreting matter (Kozlowski et al. 1978).

It is well known that all characteristic properties of the equipotential surfaces for a general rotation law are reflected by the equipotential surfaces of the simplest configurations with uniform distribution of the angular momentum density ℓ – see Jaroszyński et al. (1980). Moreover, these configurations are very important astrophysically, being marginally stable (Seguin 1975). Under the condition

$$\ell(r,\theta) = \mathrm{const}, \tag{12}$$

holding in the rotating fluid, a simple relation for the equipotential surfaces follows from Eq. (10):

$$W(r,\theta) = \ln U_t(r,\theta), \tag{13}$$

with $U_t(r,\theta)$ being determined by $\ell = \mathrm{const}$, and the metric coefficients only.

The equipotential surfaces are described by the formula $\theta = \theta(r)$, which can be given by the differential equation

$$\frac{\mathrm{d}\theta}{\mathrm{d}r} = -\frac{\partial p/\partial r}{\partial p/\partial\theta}, \tag{14}$$

which for the configurations with $\ell = \mathrm{const}$ reduces to

$$\frac{\mathrm{d}\theta}{\mathrm{d}r} = -\frac{\partial U_t/\partial r}{\partial U_t/\partial\theta}. \tag{15}$$

The influence of a non-zero cosmological constant on character of the equipotential surfaces of the marginally stable configurations rotating around a black hole will be examined in the simplest case of Schwarzschild–de Sitter spacetimes corresponding to a repulsive cosmological constant, $\Lambda > 0$. (For completeness, we briefly discuss the case of Schwarzschild––anti-de Sitter spacetimes corresponding to an attractive cosmological constant, $\Lambda < 0$.)

In the standard Schwarzschild coordinates, the non-zero metric coefficients of the Schwarzschild–(anti)-de Sitter spacetimes are

$$-g_{tt} = g_{rr}^{-1} = (1 - 2r^{-1} - yr^2), \tag{16}$$

$$g_{\theta\theta} = r^2, \tag{17}$$

$$g_{\phi\phi} = r^2\sin^2\theta. \tag{18}$$

Here, the radial coordinate r is expressed in units of the mass parameter M, and the dimensionless cosmological constant parameter

$$y = \tfrac{1}{3}\Lambda M^2 \tag{19}$$

is introduced. It should be stressed that a static region exists in the Schwarzschild–de Sitter spacetimes with subcritical values of

$$y < y_{\mathrm{c}} = \tfrac{1}{27}; \tag{20}$$

of course, the equilibrium configurations are possible only in these spacetimes. Now, the equipotential surfaces are given by the formulae

$$W(r,\theta) = \ln\frac{(1 - 2r^{-1} - yr^2)^{1/2} r\sin\theta}{\left[r^2\sin^2\theta - (1 - 2r^{-1} - yr^2)\ell^2\right]^{1/2}} \tag{21}$$

and

$$\frac{\mathrm{d}\theta}{\mathrm{d}r} = \tan\theta\,\frac{\left[r(1-yr^3)\sin^2\theta - (1-2r^{-1}-yr^2)^2\ell^2\right] r}{(r-2-yr^3)^2\ell^2}; \tag{22}$$

for $y = 0$ these relations reduce to the well known Schwarzschild formulae (Jaroszyński et al. 1980).

The best insight into the nature of the $\ell = \mathrm{const}$ configurations can be obtained by the examination of the behavior of the potential $W(r,\theta)$ in the equatorial plane ($\theta = \pi/2$). There are two reality conditions of $W(r,\theta = \pi/2)$:

$$1 - 2r^{-1} - yr^2 \geq 0, \tag{23}$$

$$r^2 - (1 - 2r^{-1} - yr^2)\ell^2 \geq 0. \tag{24}$$

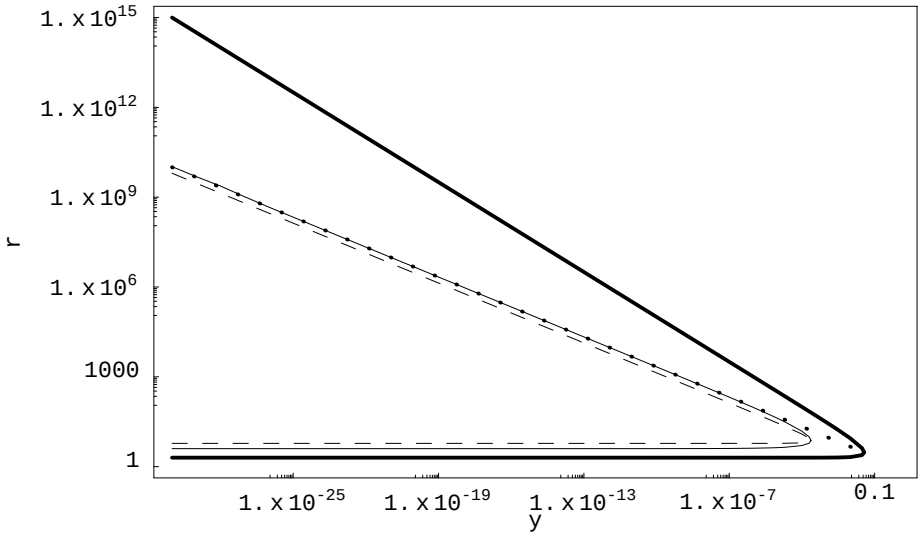

Fig. 1. Characteristic radii of the Schwarzschild–de Sitter spacetimes as functions of the parameter y. The black hole ($r_{\rm h}$) and cosmological ($r_{\rm c}$) horizons are given by bold solid lines, the static radius ($r_{\rm s}$) by bold dotted line, the radii of marginally stable orbits ($r_{\rm ms(i)}$ and $r_{\rm ms(o)}$) by thin dashed lines, and marginally bound orbits ($r_{\rm mb(i)}$ and $r_{\rm mb(o)}$) by thin solid lines.

The first condition is identical with the condition for the static regions (located between the black-hole and cosmological horizons); the second condition can be expressed in the form

$$\ell^2 \leq \ell^2_{\rm ph}(r;y) \equiv \frac{r^3}{r-2-yr^3}. \tag{25}$$

The function $\ell^2_{\rm ph}(r;y)$ is the effective potential of the photon geodesic motion; recall that $\ell \equiv U_\phi/U_t$ corresponds to the definition of the impact parameter for photon's geodesic motion – see Stuchlík & Hledík (1999). Further, the condition of the local extrema of the potential $W(r,\theta=\pi/2)$ is identical with the condition of vanishing of the pressure gradient ($\partial U_t/\partial r = 0, \partial U_t/\partial\theta = 0$). Since at the equatorial plane there is $\partial U_t/\partial\theta = 0$ independently of the $\ell = {\rm const}$, and

$$\frac{\partial U_t(r,\theta=\pi/2)}{\partial r} = \frac{\left[r(1-yr^3)-(1-2r^{-1}-yr^2)^2\ell^2\right]}{(1-2r^{-1}-yr^2)^{1/2}\left[r^2-(1-2r^{-1}-yr^2)\ell^2\right]^{3/2}}, \tag{26}$$

we arrive at the condition

$$\ell^2 = \ell^2_{\rm K}(r;y) \equiv \frac{r^3(1-yr^3)}{(r-2-yr^3)^2}. \tag{27}$$

The extrema of $W(r,\theta=\pi/2)$ correspond to the points, where the fluid moves along a circular geodesic, since $\ell^2_{\rm K}(r;y)$ corresponds to the distribution of the angular momentum density of the circular geodesic orbits. Clearly,

$$W_{\rm extr}(r,\theta=\pi/2;y) = \ln E_{\rm c}(r,y), \tag{28}$$

where

$$E_{\rm c}(r,y) = \left(1-\frac{2}{r}-yr^2\right)\left(1-\frac{3}{r}\right)^{-1/2} \tag{29}$$

is the specific energy of the circular geodesics. (Recall that the specific energy of circular geodesics corresponds to the local extrema of the effective potential $V_{\rm eff}(r;\ell,y)$ of the geodesic motion (Stuchlík & Hledík 1999).) The most important properties of the potential $W(r,\theta)$ are determined by its behavior at the equatorial plane, and, especially, by the properties of the functions $\ell^2_{\rm ph}(r;y)$, and $\ell^2_{\rm K}(r,y)$. Discussion of these properties enables us to give a classification of the Schwarzschild–(anti)-de Sitter spacetimes according to the properties of the equipotential surfaces of test perfect fluid. We shall separate the discussion to the case of the Schwarzschild–de Sitter ($y>0$), and Schwarzschild–anti-de Sitter spacetimes ($y<0$). For the pure Schwarzschild spacetime ($y=0$) the analysis can be found in (Kozlowski et al. 1978).

3.1. Schwarzschild–de Sitter black holes

If $y>0$, the function $\ell^2_{\rm ph}(r,y)$ diverges at the black-hole horizon, $r_{\rm h}$, and the cosmological horizon, $r_{\rm c}$, determined by equality in the condition (23). The horizons are given by the relations

$$r_{\rm h} = \frac{2}{\sqrt{3y}}\cos\frac{\pi+\xi}{3}, \tag{30}$$

$$r_{\rm c} = \frac{2}{\sqrt{3y}}\cos\frac{\pi-\xi}{3}, \tag{31}$$

where

$$\xi = \cos^{-1}\left(3\sqrt{3y}\right). \tag{32}$$

The radii of the horizons are illustrated in Fig. 1. The local minimum of $\ell^2_{\rm ph}(r,y)$ is located at $r_{\rm ph}=3$, independently of y, and determines the unstable photon circular geodesic with the impact parameter

$$\ell^2_{\rm ph(c)} = \ell^2_{\rm ph(min)}(y) \equiv \frac{27}{1-27y}. \tag{33}$$

The function $\ell^2_{\rm K}(r;y)$, determining the Keplerian (geodesic) circular orbits, has a zero point at the so called static radius $r_{\rm s}(y)$ given by

$$r_{\rm s} = y^{-1/3}, \tag{34}$$

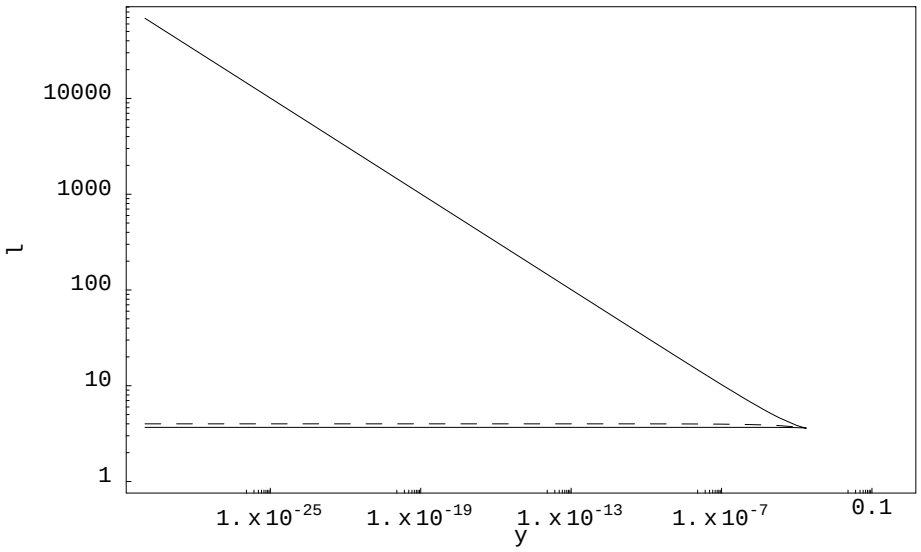

Fig. 2. The angular momentum density of the marginally stable ($\ell_{\mathrm{ms(i)}}$ and $\ell_{\mathrm{ms(o)}}$, solid line) and marginally bound (ℓ_{mb}, dashed line) orbits as functions of the parameter y of the Schwarzschild–de Sitter spacetimes. Note that $\lim_{y\to 0} \ell_{\mathrm{mb}} = 4 \neq \lim_{y\to 0} \ell_{\mathrm{ms(i)}} = 3\sqrt{3}/2$, $\lim_{y\to 0} \ell_{\mathrm{ms(o)}} = +\infty$.

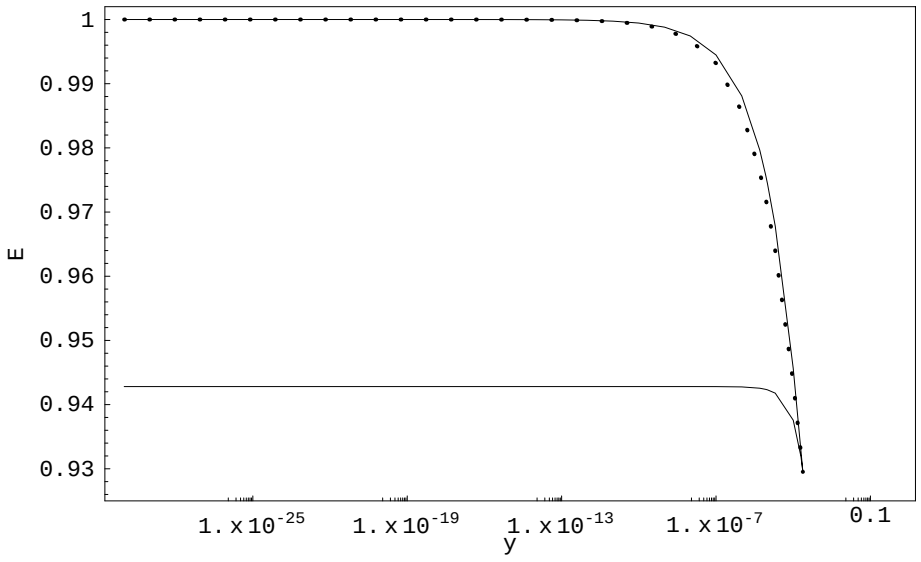

Fig. 3. The specific energy of the marginally stable ($E_{\mathrm{ms(i)}}$ and $E_{\mathrm{ms(o)}}$, solid line) and marginally bound (E_{mb}, bold dotted line) orbits as functions of the parameter y of the Schwarzschild–de Sitter spacetimes. Note that $\lim_{y\to 0} E_{\mathrm{ms(o)}} = \lim_{y\to 0} E_{\mathrm{mb}} = 1$, $\lim_{y\to 0} E_{\mathrm{ms(i)}} = 2\sqrt{2}/3$.

and it is not well defined at $r > r_{\mathrm{s}}$, being negative there. At the static radius (unstable) stationary equilibrium of test particles is possible because the gravitational attraction of the black hole is just compensated by the cosmological repulsion there.

The function $\ell^2_{\mathrm{K}}(r; y)$ diverges at the black-hole horizon: $\ell^2_{\mathrm{K}}(r \to r_{\mathrm{h}}, y) \to +\infty$; at the cosmological horizon, there is $\ell^2_{\mathrm{K}}(r \to r_{\mathrm{c}}, y) \to -\infty$. Since

$$\frac{\partial \ell^2_{\mathrm{K}}}{\partial r} = \frac{r^2[r - 6 + yr^3(15 - 4r)]}{(r - 2 - yr^3)^3}, \tag{35}$$

the local extrema of $\ell^2_{\mathrm{K}}(r, y)$ are given by the condition

$$y = y_{\mathrm{ms}}(r) \equiv \frac{r - 6}{r^3(4r - 15)}, \tag{36}$$

determining the marginally stable circular geodesics. The local maximum of $y_{\mathrm{ms}}(r)$ gives the critical value of the parameter y admitting stable circular orbits

$$y_{\mathrm{ms}} = 12/15^4 \sim 0.000237. \tag{37}$$

If $y < y_{\mathrm{ms}}$, there exists an inner (outer) marginally stable circular geodesic at $r_{\mathrm{ms(i)}}$ ($r_{\mathrm{ms(o)}}$), see Fig. 1. The angular momentum density of the marginally stable orbits $\ell_{\mathrm{ms(i)}}(y)$, and $\ell_{\mathrm{ms(o)}}(y)$, is simultaneously determined by Eqs. (27) and (36)—see Fig. 2. The specific energy of these orbits $E_{\mathrm{ms(i)}}(y)$, and $E_{\mathrm{ms(o)}}(y)$, is simultaneously determined by Eqs. (29) and (36)—see Fig. 3. There is other special value of y, corresponding to the situation, where the value of the minimum of $\ell^2_{\mathrm{ph}}(r; y)$ equals to the maximum of $\ell^2_{\mathrm{K}}(r; y)$. We denote this value y_{e}. It can be found that

$$y_{\mathrm{e}} = 1/118125 = 1/(3^3 5^4 7) \sim 0.00000846. \tag{38}$$

In the Schwarzschild–de Sitter spacetimes, there is another important class of circular geodesics—namely the marginally bound orbits. These orbits exist in the Schwarzschild–de Sitter spacetimes admitting existence of the stable circular orbits, i.e., spacetimes with $y < y_{\mathrm{ms}}$. In these spacetimes, there exists an inner, $r_{\mathrm{mb(i)}}$ (outer, $r_{\mathrm{mb(o)}}$), marginally bound orbit close to the

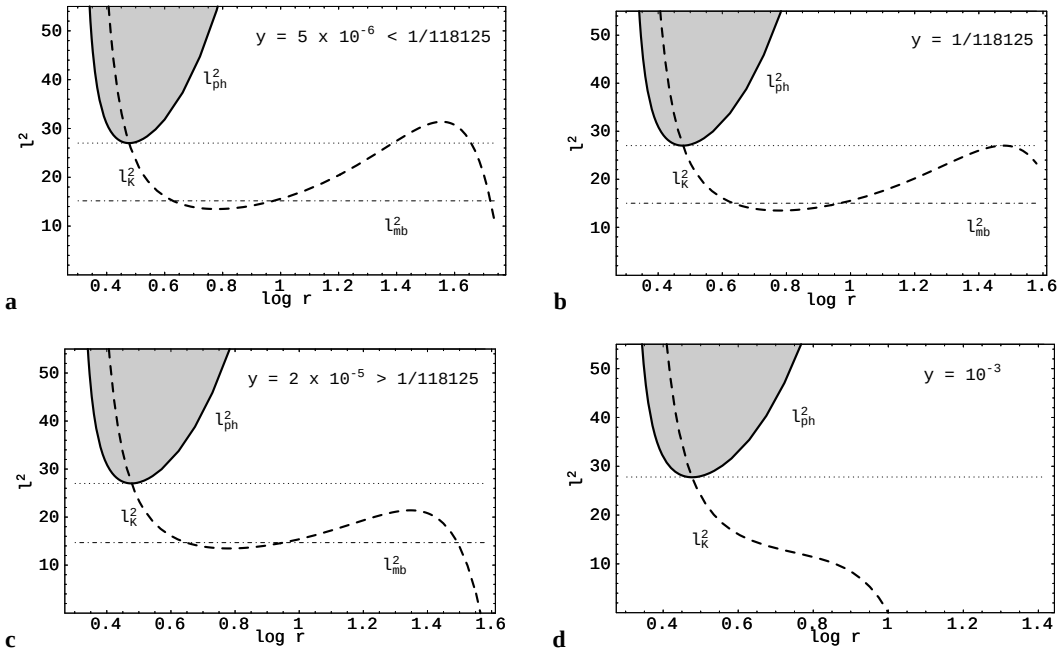

Fig. 4a–d. Behavior of the functions $\ell^2_{\rm ph}(r;y)$ and $\ell^2_{\rm K}(r;y)$ in the four qualitatively different cases determining the four classes of the Schwarzschild–de Sitter spacetimes with different properties of the equipotential surfaces (both r and ℓ^2 are given in units of M). Figures **a–d** reflect subsequently the cases $0 < y < y_{\rm e}$, $y = y_{\rm e}$, $y_{\rm e} < y < y_{\rm ms}$, and $y_{\rm ms} < y < y_{\rm c}$. In the shaded region, the equipotential surfaces are not defined in the equatorial plane of the spacetime, defined by the axis of rotation of the perfect fluid. The descending parts of the function $\ell^2_{\rm K}(r;y)$ determine the cusps, while the growing parts determine central rings of the equilibrium configurations. The dotted line ($\ell^2_{\rm ph(c)}$) determines the impact parameter of the photon circular geodesic at $r = 3$.

black-hole horizon (static radius). These orbits are defined by the condition

$$E_{\rm mb}(r_{\rm mb(i)},\ell_{\rm mb}) = E_{\rm mb}(r_{\rm mb(o)},\ell_{\rm mb}), \tag{39}$$

and are determined by an appropriate numerical procedure (see Figs. 1–3). In the Schwarzschild spacetime ($y = 0$) the marginally bound orbit is located at $r_{\rm mb} = 4$, and $E_{\rm mb} = 1$—it is because the effective potential of the geodesic motion $V_{\rm eff} \to 1$ at $r \to \infty$ independently of the angular momentum density in the Schwarzschild spacetime. In the Schwarzschild–de Sitter spacetimes with $y_{\rm ms} < y < y_{\rm c}$ the marginally bound circular orbits are not defined because only unstable circular orbits exist in these spacetimes; particles from them can always escape to infinity.

We can distinguish four qualitatively different cases of the behavior of the functions $\ell^2_{\rm ph}(r;y)$, $\ell^2_{\rm K}(r;y)$ which give four classes of the Schwarzschild–de Sitter black holes with different character of the equipotential surfaces of the rotating perfect fluid. These four classes are defined according to values of the cosmological parameter y in the following way:

(A) $0 < y < y_{\rm e}$,
(B) $y = y_{\rm e}$,
(C) $y_{\rm e} < y < y_{\rm ms}$,
(D) $y_{\rm ms} \le y < y_{\rm c}$.

For these classes, the typical behavior of the functions $\ell^2_{\rm ph}(r;y)$, $\ell^2_{\rm K}(r;y)$, with y fixed, is given in Figs. 4(a)–(d). For completeness, the corresponding value of $\ell_{\rm mb}(y)$ is exhibited in these figures. Note that the descending parts of the curve $\ell^2_{\rm K}(r;y)$ (with y fixed) correspond to the unstable circular geodesics, while its growing part (if it exists) corresponds to the stable circular geodesics. The extrema of $\ell^2_{\rm K}(r;y)$, if they exist, have an important role: the minimum $\ell_{\rm ms(i)}$, at $r_{\rm ms(i)}$, determines the inner marginally stable circular geodesic, while the maximum $\ell_{\rm ms(o)}$, at $r_{\rm ms(o)}$, determines the outer marginally stable circular geodesic.

Properties of the equipotential surfaces can be established easily, using the behavior of the potential $W(r,\theta)$ in the equatorial plane. The properties of the potential $W(r,\theta = \pi/2;y)$ are closely related to the properties of the effective potential of the geodesic motion, and at their local extrema, located at the same radii, the condition (28) is satisfied. Further, $W(r;\theta = \pi/2,y) \to -\infty$, if $r \to r_{\rm h}$ or $r \to r_{\rm c}$. The topological properties of the equipotential surfaces can be directly inferred from the properties of the potential $W(r,\theta = \pi/2;y)$. The local extrema of the potential $W(r,\theta = \pi/2;y)$ are determined by the condition

$$\ell^2 = \ell^2_{\rm K}(r;y); \tag{40}$$

therefore, at the radii determined by the local extrema of $W(r,\theta = \pi/2;y)$, perfect fluid follows free, geodesic circular orbits. The maxima of the potential are determined by the descending part of $\ell^2_{\rm K}(r;y)$, they correspond to the cusps of the equipotential surfaces, and the matter moves along an unstable geodesic orbit at the corresponding radii. The minima of the potential are determined by the rising part of $\ell^2_{\rm K}(r;y)$,

they correspond to the central rings of the equilibrium configurations, and the matter moves along a stable geodesic orbit at the corresponding radii.

Now, we give a complete survey of the behavior of the equipotential surfaces, and the related potential $W(r,\theta=\pi/2;y)$. We start with the astrophysically most important case.

(A) $\mathbf{0 < y < y_e}$. From Fig. 4a, we obtain nine qualitatively different cases of the behavior of the potential $W(r,\theta=\pi/2)$, and corresponding nine qualitatively different families of the equipotential surfaces, according to the values of $\ell = \mathrm{const}$. (In the following, we consider $\ell > 0$ only. This can be done due to the symmetry of the spacetimes under consideration.)
- (I) $\ell < \ell_{\mathrm{ms(i)}}$. Open surfaces only; no disks are possible. Surface with the outer cusp exists. (Fig. 5a)
- (II) $\ell = \ell_{\mathrm{ms(i)}}$. An infinitesimally thin, unstable ring located at $r_{\mathrm{ms(i)}}$ exists. An open surface with the outer cusp exists. (Fig. 5b)
- (III) $\ell_{\mathrm{ms(i)}} < \ell < \ell_{\mathrm{mb}}$. Closed surfaces exist. Many equilibrium configurations without cusps are possible, and one with the inner cusp. An open surface with the outer cusp exists. (Fig. 5c)
- (IV) $\ell = \ell_{\mathrm{mb}}$. Many equilibrium configurations without cusps are possible. There is an equipotential surface with both the inner and outer cusps. Now, the mechanical nonequilibrium causes an inflow into the black hole, and an outflow from the disk, with the same efficiency; it is the most interesting new feature of the accretion processes caused by the presence of a repulsive cosmological constant. (Fig. 5d)
- (V) $\ell_{\mathrm{mb}} < \ell < \ell_{\mathrm{ph(c)}}$. Equilibrium configurations are possible because closed equipotential surfaces exist. However, accretion into the black hole is impossible because the equilibrium configurations (closed surfaces) have no inner cusp; the inner cusp has an open equipotential surface. The outer cusp belongs to a closed surface, and the outflow from the disk is possible. (Fig. 5e)
- (VI) $\ell = \ell_{(\mathrm{ph(c)})}$. The potential $W(r,\theta=\pi/2;y)$ diverges at the photon circular orbit located at $r=3$, and the inner cusp disappears. The closed equipotential surfaces still exist, with the most extended one containing the outer cusp that enables outflow from the disk. (Fig. 5f)
- (VII) $\ell_{\mathrm{ph(c)}} < \ell < \ell_{\mathrm{ms(o)}}$. In the region defined by $\ell^2_{\mathrm{ph}}(r;y)$, the equipotential surfaces cannot reach the equatorial plane. The closed equipotential surfaces exist, one with the outer cusp. (Fig. 5g)
- (VIII) $\ell = \ell_{\mathrm{ms(o)}}$. An infinitesimally thin, unstable ring located at $r_{\mathrm{ms(o)}}$ exists (the center, and the outer cusp coalesce). (Fig. 5h)
- (IX) $\ell > \ell_{\mathrm{ms(o)}}$. Open equipotential surfaces exist only. There is no cusp in this case. (Fig. 5i).

(B) $\boldsymbol{y = y_e}$. For this special value of y (Fig. 4b), we still obtain the families of equipotential surfaces given by (A-I)–(A-V) and (A-IX). However, the case (A-VII) disappears, and the cases (A-VI) and (A-VIII) coalesce, giving the case
- (X) $\ell = \ell_{\mathrm{ph(c)}} = \ell_{\mathrm{ms(o)}}$. The inner cusp just disappears, while the outer cusp coalesce with the center. (Fig. 5j)

(C) $\mathbf{y_e < y < y_{ms}}$. From Fig. 4c it follows that the intervals of ℓ, and the families of equipotential surfaces (A-I)–(A-IV) remain. The following new intervals of the angular momentum density must be introduced.
- (XI) $\ell_{\mathrm{mb}} < \ell < \ell_{\mathrm{ms(o)}}$. This case is equivalent to the case (A-V).
- (XII) $\ell = \ell_{\mathrm{ms(o)}}$. There is the inner cusp of an open equipotential surface, but the center and the outer cusp coalesce—this corresponds to an infinitesimally thin unstable ring, located at $r_{\mathrm{ms(o)}}$. (Fig. 5k)
- (XIII) $\ell_{\mathrm{ms(o)}} < \ell < \ell_{\mathrm{ph(c)}}$. There are open surfaces only, one being with the inner cusp. (Fig. 5l)
- (XIV) $\ell \geq \ell_{\mathrm{ph(c)}}$. This case corresponds to the case (A-IX).

(D) $\mathbf{y_{ms} \leq y < y_c}$. For this interval of y, the function $\ell^2_{\mathrm{K}}(r;y)$ is descending everywhere (see Fig. 4d). Only maxima of the potential $W(r,\theta=\pi/2;y)$ are possible (if $\ell^2 < \ell^2_{\mathrm{ph(c)}}$), and open equipotential surfaces can exist only. Equilibrium configurations corresponding to toroidal disks are not possible. This is quite natural result, since in the spacetimes under consideration stable circular geodesics cannot exist. Now, there are only two different intervals of the parameter ℓ.
- (XV) $\ell < \ell_{\mathrm{ph(c)}}$. This family of equipotential surfaces corresponds to the case (A-I).
- (XVI) $\ell \geq \ell_{\mathrm{ph(c)}}$. This family of equipotential surfaces corresponds to the case (A-IX).

Values of the potential at the central ring and the cusps (provided they exist) are given in Table 1. Note that the maximum difference between the values of the potential W on the boundary and at the center of the toroidal disk in the Schwarzschild spacetime is $\Delta W = 0.0431$ (Abramowicz et al. 1978). Comparing this with the value $\Delta W_{\mathrm{i}} = \Delta W_{\mathrm{o}} = 0.0309$ from Table 1 characterizing the limiting accretion disk with $\ell = \ell_{\mathrm{mb}}$, we can conclude that the presence of a repulsive cosmological constant makes the structure of the disk 'smoother'.

The Schwarzschild case $y = 0$ was discussed in (Kozlowski et al.1978) and will not be repeated here. We only mention that the critical self-crossing surface for the marginally bound configurations $W_{\mathrm{cusp}}(\ell = \ell_{\mathrm{mb}}; y = 0) = 0$, while $W_{\mathrm{cusp}}(\ell = \ell_{\mathrm{mb}}, y > 0) < 0$.

3.2. Schwarzschild–anti-de Sitter black holes

If $y < 0$, the function $\ell^2_{\mathrm{ph}}(r,y)$ diverges at infinity, and at the black-hole horizon given by the relation

$$r_{\mathrm{h}} = \left[-\frac{1}{y} + \left(\frac{1}{y^2} - \frac{1}{27y^3}\right)^{1/2}\right]^{1/3} + \left[-\frac{1}{y} - \left(\frac{1}{y^2} - \frac{1}{27y^3}\right)^{1/2}\right]^{1/3}. \quad (41)$$

The local minimum of $\ell^2_{\mathrm{ph}}(r;y)$ is again located at $r_{\mathrm{ph}} = 3$, and the impact parameter of the corresponding photon cir-

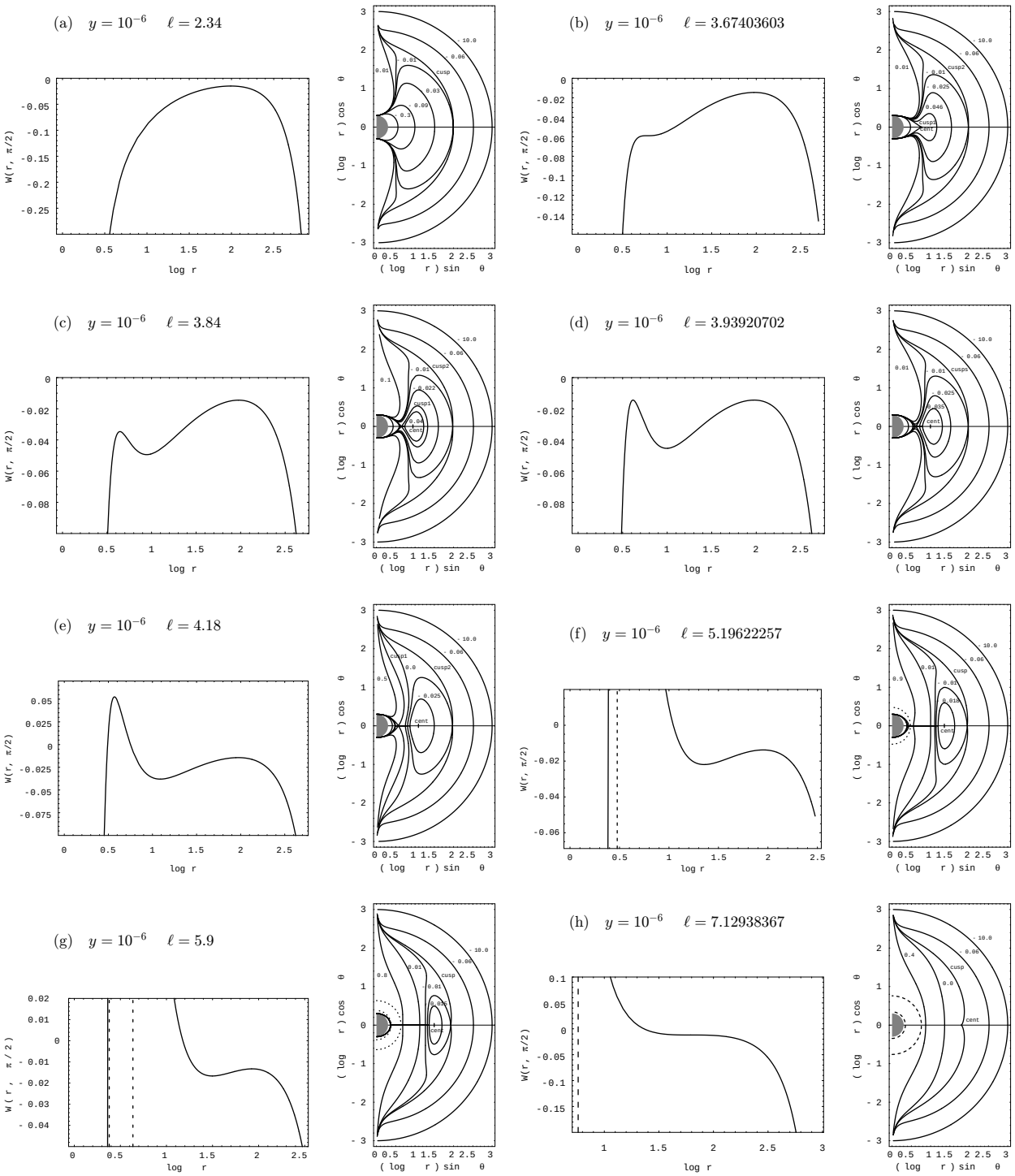

Fig. 5a–h. Equipotential surfaces (meridional sections) for the marginally stable ($\ell = \mathrm{const}$) configurations of test perfect fluid orbiting the Schwarzschild–de Sitter black-holes, and the related potential $W(r, \theta = \pi/2; y)$. The radial coordinate is expressed in units of M; the logarithmic scale is used, in order to cover whole the range between the inner and outer cusps. The central black hole is shaded. The sequence of figures **a–l** covers all the possibilities of the behavior of the equipotential surfaces for black holes in spacetimes with a repulsive cosmological constant. The sequence **a–i** gives successively all the possibilities for the behavior of the equipotential surfaces in the spacetimes of class A, with $0 < y < y_{\mathrm{e}}$, which is the astrophysically most plausible class. For the spacetimes of the classes B–D, the relevant sequences of the equipotential surfaces are determined in the text. The cusps of the toroidal disks correspond to the local maxima of $W(r, \theta = \pi/2)$, the central rings correspond to their local minima. The dashed lines give asymptotics of $W(r, \theta = \pi/2)$, and determine the interval of radii where the equipotential surfaces cannot reach the equatorial plane.

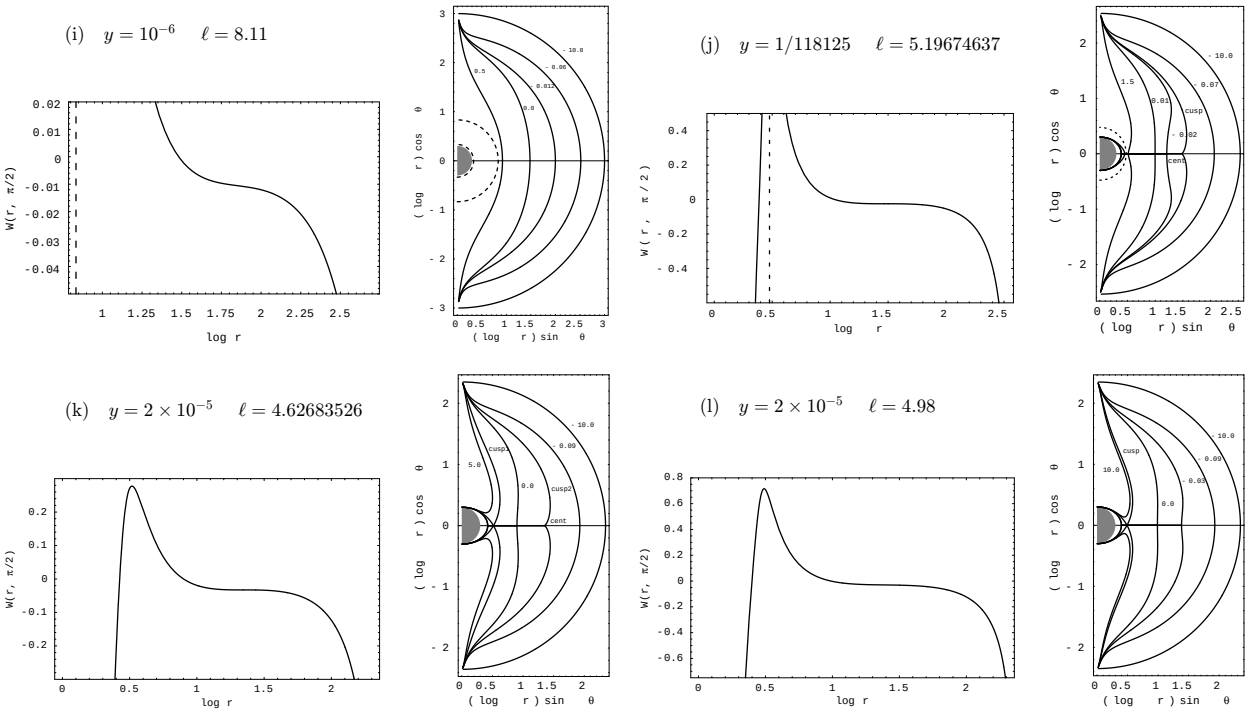

Fig. 5i–l.

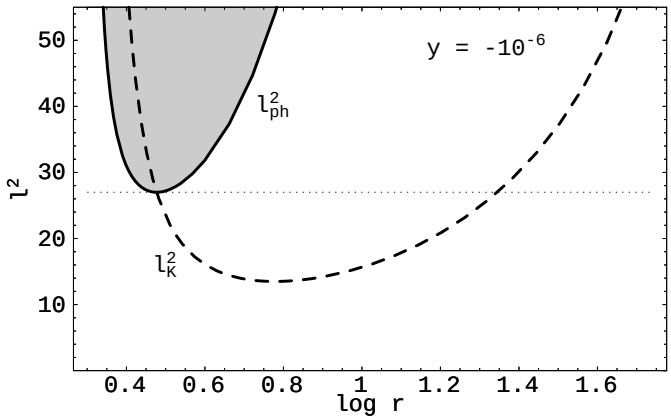

Fig. 6. Behavior of the functions $\ell^2_{\rm ph}(r;y)$ and $\ell^2_{\rm K}(r;y)$ for the Schwarzschild–anti-de Sitter spacetimes, given for $y = -10^{-6}$ (both r and ℓ^2 are given in units of M). The dotted line determines $\ell^2_{\rm ph(c)}$, as in Fig. 4. It is qualitatively similar to the pure Schwarzschild case ($y = 0$), and it has the same character for all $y < 0$. In the shaded region, the equipotential surfaces are not defined in the equatorial plane.

cular geodesic is given by Eq. (33). If $y < 0$, there is no zero point of $\ell^2_{\rm K}(r, y)$ and $\ell^2_{\rm K}(r \to r_{\rm h}, y) \to +\infty$, $\ell^2_{\rm K}(r \to \infty, y) \to +\infty$. Now, Eq. (36) determines only one marginally stable circular geodesic, close to the horizon. On the other hand, in the Schwarzschild–anti-de Sitter spacetimes the notion of marginally bound circular geodesic ceases any meaning because particles from the unstable circular orbits never escape to infinity, since the effective potential diverges at infinity for each value of the angular momentum density (Stuchlík & Hledík 1999).

If $y < 0$, the behavior of the functions $\ell^2_{\rm ph}(r;y)$ and $\ell^2_{\rm K}(r;y)$ is qualitatively the same as in the Schwarzschild case. It is illustrated in Fig. 6. The function $\ell^2_{\rm K}(r;y)$ has a minimum $\ell_{\rm ms}$ at $r_{\rm ms}$ corresponding to the marginally stable circular geodesic. The unstable geodesics are given by the descending part of $\ell^2_{\rm K}(r;y)$, while the stable are given by the rising part.

Now, it is immediately clear that for all of the Schwarzschild–anti-de Sitter spacetimes we always obtain four possible cases of the behavior of the potential $W(r, \theta = \pi/2; y)$ and four corresponding families of the equipotential surfaces; notice that $W(r, \theta = \pi/2, y) \to \infty$ as $r \to \infty$. These cases are given by the following intervals of ℓ:

(I) $\ell < \ell_{\rm ms}$. There are open equipotential surfaces only. (Fig. 7a)

(II) $\ell = \ell_{\rm ms}$. An infinitesimally thin unstable ring is located at $r_{\rm ms}$. (Fig. 7b)

(III) $\ell_{\rm ms} < \ell \leq \ell_{\rm ph(c)}$. Closed equipotential surfaces exist, one with the cusp that enables accretion from the toroidal disk into the black hole. (Fig. 7c)

(IV) $\ell > \ell_{\rm ph(c)}$. Closed equipotential surfaces exist, but no with a cusp at the equatorial plane. In vicinity of the horizon (in region limited by radii determined by the equation $\ell^2_{\rm ph}(r;y) = \ell^2$) the equipotential surfaces cannot cross the equatorial plane. (Fig. 7d)

Values of the potential at the cusp and the central ring (provided they exist) are given in Table 2.

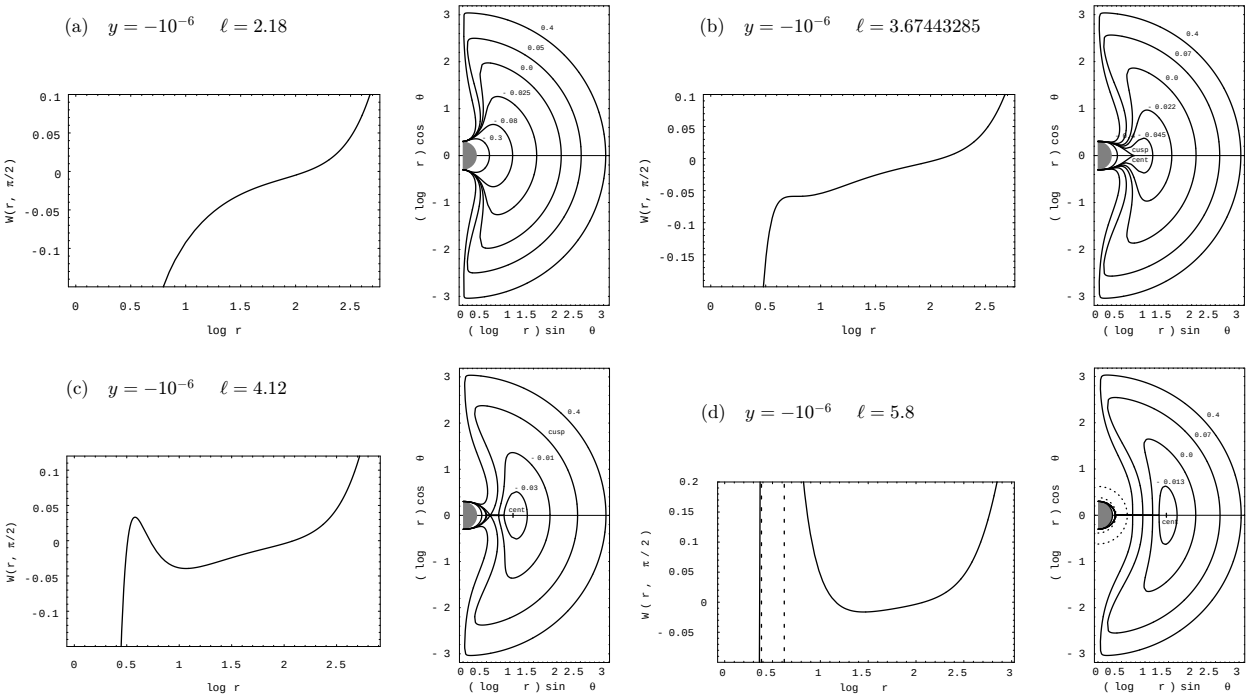

Fig. 7a–d. Equipotential surfaces (meridional sections) for the marginally stable ($\ell = \text{const}$) configurations of test perfect fluid orbiting the Schwarzschild–anti-de Sitter black holes, and the related potential $W(r, \theta = \pi/2, y)$, given for $y = -10^{-6}$. The behavior of the equipotential surfaces has the same character for all $y < 0$. There are four possibilities described in the text. We express the radial coordinate in units of M, and use the logarithmic scale. The central black hole is shaded. Notice the special shape of the equipotential surfaces with a cusp, resembling a falling wave. The dashed lines give asymptotics of $W(r, \theta = \pi/2)$, and determine the interval of radii where the equipotential surfaces cannot reach the equatorial plane.

Table 1. Radii of the inner cusp ($r_{\mathrm{cu(i)}}$), outer cusp ($r_{\mathrm{cu(o)}}$), and the central ring (r_{cent}), the corresponding values of the potential ($W_{\mathrm{cu(i)}}$, $W_{\mathrm{cu(o)}}$, W_{cent}), and the differences ($\Delta W_{\mathrm{i}} = W_{\mathrm{cu(i)}} - W_{\mathrm{cent}}$, $\Delta W_{\mathrm{o}} = W_{\mathrm{cu(o)}} - W_{\mathrm{cent}}$) for the equilibrium configurations with $\ell = \text{const}$ in the Schwarzschild–de Sitter spacetimes. (Radii and ℓ are in units of mass parameter M, while W and ΔW are in units of c^2.)

y	ℓ	$r_{\mathrm{cu(i)}}$	r_{cent}	$r_{\mathrm{cu(o)}}$	$W_{\mathrm{cu(i)}}$	W_{cent}	$W_{\mathrm{cu(o)}}$	ΔW_{i}	ΔW_{o}
10^{-6}	2.3400	none	none	98.2201	none	none	-0.01496	none	none
10^{-6}	3.6740	6.00195	6.00195	95.3473	-0.05895	-0.05895	-0.01454	0	0.04410
10^{-6}	3.8400	4.41949	8.82178	94.8669	-0.03464	-0.04940	-0.01448	0.01476	0.03492
10^{-6}	3.9392	4.13295	9.87591	94.5644	-0.01443	-0.04537	-0.01443	0.03094	0.03094
10^{-6}	3.9900	4.02028	10.3897	94.4048	-0.00251	-0.04358	-0.01441	0.04107	0.02917
10^{-6}	4.1800	3.70860	12.2516	93.7790	0.05255	-0.03797	-0.01433	0.09052	0.02364
10^{-6}	5.1962	3	22.6904	89.4730	∞	-0.02193	-0.01378	∞	0.00815
10^{-6}	5.9000	none	31.4330	85.0665	none	-0.01664	-0.01328	none	0.00337
10^{-6}	7.1294	none	62.1768	62.1768	none	-0.01197	-0.01197	none	0
10^{-6}	8.1100	none	none	none	none	none	none	none	none
2×10^{-5}	4.6268	3.29004	22.2247	22.2247	0.27754	-0.03271	-0.03271	0.31025	0
2×10^{-5}	4.9800	3.09207	none	none	0.71569	none	none	none	none
10^{-3}	2.1800	none	none	9.06615	none	none	-0.15977	none	none
$1/118125$	5.1967	3	30	30	∞	-0.02451	-0.02451	∞	0

4. Conclusions

The new phenomena in the structure of equilibrium configurations of test perfect fluid, caused by the presence of a repulsive cosmological constant, can be summarized in the following way.

1. There is always an equipotential surface with a cusp for $\ell = 0$. It is always an open surface.
2. The position of the outer cusp of the equipotential surface with $\ell = 0$ is just at $r_{\mathrm{cusp}}(\ell = 0) = r_{\mathrm{s}} = \sqrt[3]{1/y}$. The value of the potential at the cusp is given by

$$W_{\mathrm{max}}(r_{\mathrm{s}}, \ell = 0, y) = \ln E_{\mathrm{c}}(r_{\mathrm{s}}, \ell = 0, y). \tag{42}$$

Because

$$E_{\mathrm{c}}(r = r_{\mathrm{s}}, \ell = 0, y) = \left(1 - 3y^{1/3}\right)^{1/2}, \tag{43}$$

Table 2. Radii of the cusp and central ring, the corresponding values of the potential and their difference for equilibrium configurations with $\ell = \mathrm{const}$ in the Schwarzschild–anti-de Sitter spacetimes.

y	ℓ	$r_{\mathrm{cu(i)}}$	r_{cent}	$r_{\mathrm{cu(o)}}$	$W_{\mathrm{cu(i)}}$	W_{cent}	$W_{\mathrm{cu(o)}}$	ΔW_{i}	ΔW_{o}
-10^{-6}	2.1800	none	none	none	none	none	none	none	none
-10^{-6}	3.6744	5.99806	5.99806	none	-0.05884	-0.05884	none	0	none
-10^{-6}	4.1200	3.79293	11.6194	none	0.03332	-0.03940	none	0.07272	none
-10^{-6}	5.8000	none	28.4736	none	none	-0.01629	none	none	none

we find

$$W_{\mathrm{cusp}}(\ell = 0) = \frac{1}{2}\ln\left(1 - 3y^{1/3}\right). \tag{44}$$

3. The accretion disks around black holes can exist when an inner cusp will appear near the black-hole horizon, in addition to the outer cusp, located nearby the static radius $r_{\mathrm{s}} = \sqrt[3]{1/y}$.
4. Closed equipotential surfaces, necessary for the existence of toroidal accretion disks, can exist for $\ell \in (\ell_{\mathrm{ms(i)}}, \ell_{\mathrm{ms(o)}})$. Here $\ell_{\mathrm{ms(i)}}$ ($\ell_{\mathrm{ms(o)}}$) corresponds to the local minimum (maximum) of the function $\ell^2_{\mathrm{K}}(r; y)$, giving the minimum (maximum) value ℓ of stable circular geodesic (Keplerian) orbits. The closed surfaces can exist in the spacetimes with $y < y_{\mathrm{ms}} \sim 0.000237$.
5. Accretion onto the central black hole by the Paczyński mechanism is possible, if $\ell \in (\ell_{\mathrm{ms(i)}}, \ell_{\mathrm{mb}})$; The value ℓ_{mb} corresponds to the marginally bound circular geodesics. Now, they are determined nontrivially: by the condition that for $\ell = \ell_{\mathrm{mb}}$ both $W(r, \theta = \pi/2)$ and the effective potential of geodesic motion $V_{\mathrm{eff}}(r; \ell_{\mathrm{mb}}, y)$ have two local maxima with the same value (recall that $W_{\mathrm{max}}(r, \theta = \pi/2) = \ln V_{\mathrm{eff(max)}}$ there). In this case, outflow from the accretion disk is possible through both cusps, if the mechanical equilibrium is destroyed for both the cusps, i.e., if both equipotential surfaces with cusp are filled up: $W > W_{\mathrm{cusp(o)}} > W_{\mathrm{cusp(i)}}$. If $W_{\mathrm{cusp(i)}} < W < W_{\mathrm{cusp(o)}}$, the accretion flow is directed down the black hole only.
6. We stress that for $\ell = \ell_{\mathrm{mb}}$, the equipotential surface with $W = W_{\mathrm{max}}(r_{\mathrm{mb(i)}}, y) = W_{\mathrm{max}}(r_{\mathrm{mb(o)}}, y)$ has two cusps. The mass outflow due to mechanical non-equilibrium, i.e., overfilling of the (both-sided) marginally closed equipotential surface, is equally efficient for the inflow down the black hole and the outflow near the static radius. Of course, we could expect significant differences in details of the accretion inflow near the black-hole horizon, and the outflow near the static radius.
7. The outer cusp of the configuration with $\ell = \ell_{\mathrm{mb}}$, and $W_{\mathrm{cusp}} = \ln E_{\mathrm{mb}}$, i.e., the limiting equilibrium configuration which enables accretion into the Schwarzschild–de Sitter black holes, is located at $r = r_{\mathrm{mb(o)}}$. It is quite interesting that such configurations will approach the static radius, however, they cannot exceed the static radius ($r_{\mathrm{mb(o)}} \to r_{\mathrm{s}}$ if $y \to 0$). Notice that $\ell_{\mathrm{mb}} \sim \ell_{\mathrm{ms(i)}}$ (Fig. 2), while $E_{\mathrm{mb}} \sim E_{\mathrm{ms(o)}}$ (Fig. 3).
8. For $\ell \in (\ell_{\mathrm{mb}}, \ell_{\mathrm{ms(o)}})$, the accretion flow down the hole is "switched-off", because an open self–crossing equipotential surface with $W = W_{\mathrm{cusp(i)}}$ appears under the inner edge of the toroidal configuration in the equatorial plane. However, the outflow through the cusp near the static radius can still occur due to a possible mechanical non-equilibrium.
9. Toroidal structures of equipotential surfaces, leading to equilibrium configurations of perfect fluid, cannot exist just if $\ell > \ell_{\mathrm{ms(o)}}$. Then, an inner cusp, nearby the black-hole horizon, still exists for equipotential surfaces with $W = W_{\mathrm{cusp(i)}} > 0$. However, these equipotential surfaces are always open, and can exist in spacetimes with $y_{\mathrm{e}} < y < y_{\mathrm{c}}$.
10. The behavior of the open equipotential surfaces along the axis of rotation gives an important effect—the surfaces become significantly narrower while approaching the static radius and the cosmological horizon. This behavior suggests a strong collimation effect on jets, caused by the influence of a repulsive cosmological constant.

In the case of Schwarzschild–anti-de Sitter spacetimes the situation is different. The presence of an attractive cosmological constant brings no qualitatively new phenomena in comparison with the Schwarzschild case, concerning the character of the equilibrium configurations related to accretion disks. Notice, however, the special shape (resembling a falling wave) of the closed equipotential surfaces which manifests in an illustrative way the interplay of the gravitational, cosmological, and centrifugal forces. Moreover, there exist no open equipotential surfaces around the rotation axis in these spacetimes.

From the astrophysical point of view, the most important phenomena were discovered in spacetimes with a repulsive cosmological constant, if they admit stable circular geodesic orbits. The first is the presence of an outer cusp of toroidal disks nearby the static radius which enables outflow of mass and angular momentum from the accretion disks by the Paczyński mechanism, i.e., due to a violation of the hydrostatic equilibrium. This is the same mechanism that drives the accretion into the black hole through the inner cusp. (Recall that outflow from toroidal disks around a Schwarzschild or Kerr black hole by the Paczyński mechanism is impossible because no outer cusp of toroidal disks exists in the asymptotically flat black-hole spacetimes (Kozlowski et al. 1978; Abramowicz et al. 1978; Jaroszyński et al. 1980).) The second is the possibility of strong collimation effects on jets escaping along the rotation axis of toroidal disks following the open equipotential surfaces that are narrowing strongly when approaching the static radius (and the cosmological horizon). We give an explicit illustration of these two principally new phenomena caused by the repulsive cosmolog-

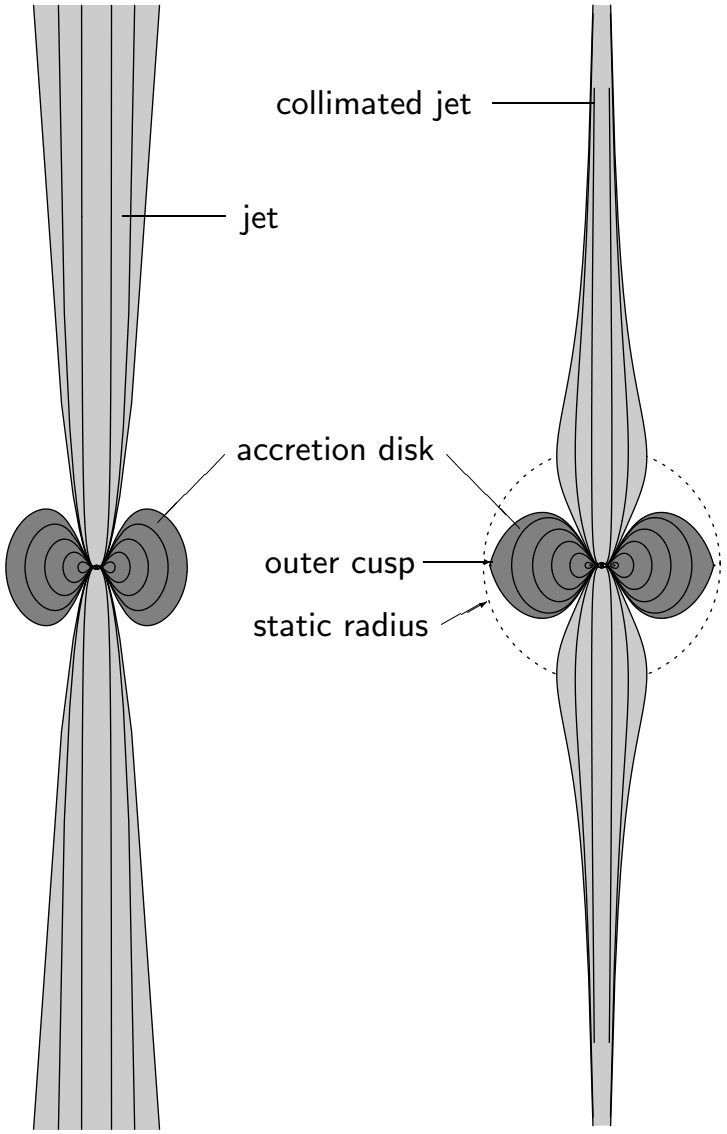

Thick accretion disk around a Schwarzschild black hole, $y = 0$, $\ell(r, \vartheta) = 3.96 < \ell_{\rm mb}$

Thick accretion disk around a Schwarzschild–de Sitter black hole, $y = 10^{-6}$, $\ell(r, \vartheta) = {\rm const} = \ell_{\rm mb}$

Fig. 8. The structure of an accretion disk with a jet is compared in meridian sections. The radial coordinate is expressed in units of M, but the logarithmic scale is not used here, since we are interested in the regions near the static radius where both the outer cusp and the collimation effect are evident.

ical constant in Fig. 8. Of course, both of those very interesting phenomena deserve further, more detailed studies. Further, the runaway instability of the toroidal disks with respect to the outflow through the outer cusp, and the influence of self–gravitation on their structure, have to be examined. We plan these studies in near future.

It is interesting to find astrophysically plausible situations in which these two phenomena could be relevant. We should consider their role in

(a) quasars and active galactic nuclei during the present period of expansion of the Universe,

(b) accretion processes onto primordial black holes during the very early stages of expansion of the Universe, when phase transitions connected to symmetry breaking of physical interactions due to Higgs mechanism (e.g., the breaking of electroweak interactions) could take place, and the effective cosmological constant can have values in many orders exceeding its present value (Kolb & Turner 1990).

Recent cosmological observations give strong indications that the present value of the vacuum energy density is (Krauss 1998)

$$\rho_{\rm vac(0)} \approx 0.65 \rho_{\rm crit(0)} \tag{45}$$

Table 3. Characteristic radii of the Schwarzschild–de Sitter black-hole spacetimes (in units of mass parameter M). The parameter $S = r_{\mathrm{mb(o)}}/r_{\mathrm{mb(i)}}$ determines the relative extension of the toroidal accretion disks with $\ell = \mathrm{const} = \ell_{\mathrm{mb}}$. The table ends at $y = y_{\mathrm{ms}} \sim 0.000237$, corresponding to the marginal spacetime allowing stable circular geodesics. In spacetimes with $y > y_{\mathrm{ms}}$, stable circular geodesics are not allowed, and both thick and thin accretion disks cannot exist.

y	r_{h}	r_{c}	r_{s}	$r_{\mathrm{ms(i)}}$	$r_{\mathrm{ms(o)}}$	$r_{\mathrm{mb(i)}}$	$r_{\mathrm{mb(o)}}$	S
1×10^{-30}	2	1×10^{15}	1×10^{10}	6	6.30×10^{9}	4	1×10^{10}	1.05×10^{9}
1×10^{-29}	2	3.16×10^{14}	4.64×10^{9}	6	2.92×10^{9}	4	4.64×10^{9}	4.87×10^{8}
1×10^{-28}	2	1×10^{14}	2.15×10^{9}	6	1.36×10^{9}	4	2.15×10^{9}	2.26×10^{8}
1×10^{-27}	2	3.16×10^{13}	1×10^{9}	6	6.30×10^{8}	4	1×10^{9}	1.05×10^{8}
1×10^{-26}	2	1×10^{13}	4.64×10^{8}	6	2.92×10^{8}	4	4.64×10^{8}	4.87×10^{7}
1×10^{-25}	2	3.16×10^{12}	2.15×10^{8}	6	1.36×10^{8}	4	2.15×10^{8}	2.26×10^{7}
1×10^{-24}	2	1×10^{12}	1×10^{8}	6	6.30×10^{7}	4	1×10^{8}	1.05×10^{7}
1×10^{-23}	2	3.16×10^{11}	4.64×10^{7}	6	2.92×10^{7}	4	4.64×10^{7}	4.87×10^{6}
1×10^{-22}	2	1×10^{11}	2.15×10^{7}	6	1.36×10^{7}	4	2.15×10^{7}	2.26×10^{6}
1×10^{-21}	2	3.16×10^{10}	1×10^{7}	6	6.30×10^{6}	4	1×10^{7}	1.05×10^{6}
1×10^{-20}	2	1×10^{10}	4.64×10^{6}	6	2.92×10^{6}	4	4.64×10^{6}	4.87×10^{5}
1×10^{-19}	2	3.16×10^{9}	2.15×10^{6}	6	1.36×10^{6}	4	2.15×10^{6}	2.26×10^{5}
1×10^{-18}	2	1×10^{9}	1×10^{6}	6	6.30×10^{5}	4	1×10^{6}	1.05×10^{5}
1×10^{-17}	2	3.16×10^{8}	4.64×10^{5}	6	2.92×10^{5}	4	4.64×10^{5}	4.87×10^{4}
1×10^{-16}	2	1×10^{8}	2.15×10^{5}	6	1.36×10^{5}	4	2.15×10^{5}	2.26×10^{4}
1×10^{-15}	2	3.16×10^{7}	1×10^{5}	6	6.30×10^{4}	4	1×10^{5}	1.05×10^{4}
1×10^{-14}	2	1×10^{7}	4.64×10^{4}	6	2.92×10^{4}	4	4.64×10^{4}	4.87×10^{3}
1×10^{-13}	2	3.16×10^{6}	2.15×10^{4}	6	1.36×10^{4}	4	2.15×10^{4}	2.26×10^{3}
1×10^{-12}	2	1×10^{6}	1×10^{4}	6	6.30×10^{3}	4.001	1×10^{4}	1.05×10^{3}
1×10^{-11}	2	3.16×10^{5}	4.64×10^{3}	6	2.92×10^{3}	4.003	4.64×10^{3}	4.87×10^{2}
1×10^{-10}	2	1×10^{5}	2.15×10^{3}	6	1.36×10^{3}	4.006	2.15×10^{3}	2.26×10^{2}
1×10^{-9}	2	3.16×10^{4}	1×10^{3}	6	6.30×10^{2}	4.012	9.95×10^{2}	1.05×10^{2}
1×10^{-8}	2	1×10^{4}	4.64×10^{2}	6	2.92×10^{2}	4.026	4.59×10^{2}	48.6
1×10^{-7}	2	3.16×10^{3}	2.15×10^{2}	6	1.36×10^{2}	4.058	2.10×10^{2}	22.5
1×10^{-6}	2	1×10^{3}	1×10^{2}	6.002	62.2	4.132	9.46	10.4
5×10^{-6}	2	4.46×10^{2}	58.5	6.01	36.0	4.247	53.0	5.98
8.466×10^{-6}	2	3.43×10^{2}	49.1	6.02	30.0	4.306	43.5	4.99
1×10^{-5}	2.0001	3.16×10^{2}	46.4	6.02	28.3	4.328	40.8	4.70
2×10^{-5}	2.0002	2.23×10^{2}	36.8	6.04	22.2	4.446	31.1	3.68
1×10^{-4}	2.0008	1×10^{2}	21.5	6.24	12.2	5.082	15.3	1.96
2×10^{-4}	2.0016	70	17.1	6.72	8.89	6.097	9.84	1.32
2.370×10^{-4}	2.0019	64	16.2	7.50	7.50	7.568	7.568	1

with present values of the critical energy density $\rho_{\mathrm{crit}(0)}$, and Hubble parameter H_0 given by

$$\rho_{\mathrm{crit}(0)} = \frac{3H_0^2}{8\pi}, \quad H_0 = 100h\,\mathrm{km\,s^{-1}\,Mpc^{-1}}. \tag{46}$$

Taking value of the dimensionless parameter $h \sim 0.7$, we arrive at the present value of the "relict" repulsive cosmological constant

$$\Lambda_0 = 8\pi\rho_{\mathrm{vac}(0)} \approx 1.1\times10^{-56}\,\mathrm{cm^{-2}}. \tag{47}$$

Having this value of Λ_0, we can determine the mass parameter of the spacetime corresponding to any given value of y, and all the relevant parameters of the equilibrium configurations. The results concerning the important radii characterizing the Schwarzschild–de Sitter spacetimes with $\Lambda = \Lambda_0$ are summarized in Table 3 and Table 4.

We can clearly see that the relict cosmological constant $\Lambda_0 \sim 1.1\times10^{-56}\,\mathrm{cm^{-2}}$ puts a natural limit on the size of equilibrium configurations rotating around black holes. In fact, the outer edge of the accretion disks, where the outflow goes through the outer cusp of the toroidal structure, is located nearby the static radius. It is quite interesting that for black holes of masses $\sim10^8 M_\odot$–$10^9 M_\odot$, corresponding to black holes located in the central parts of quasars and active galactic nuclei, the outer edge of the largest accretion disks is located at $r_{\mathrm{mb(o)}} \sim 50$–$100$ kpc, and is comparable with maximum extension of large galaxies. Note that extension of quasikeplerian, thin accretion disks is limited by the outer marginally stable circular orbit; if y is small enough ($y \leq 10^{-8}$), it can be shown that

$$r_{\mathrm{ms(o)}} \sim 0.63 r_{\mathrm{s}}, \tag{48}$$

and dimensions of these disks are comparable to the static radius, too. Therefore, the relict repulsive cosmological constant can radically influence the behavior of accretion disks in large galaxies with active nuclei, and can even be connected to the limit of extension of these large galaxies.

Moreover, it is clear that the collimation effect of the repulsive cosmological constant could be relevant in these situations,

Table 4. Mass parameter and the radius $r_{\mathrm{mb(o)}}$ determining the outer edge of toroidal disks with $\ell = \mathrm{const} = \ell_{\mathrm{mb}}$ in the Schwarzschild–de Sitter black-hole spacetimes, given for (a) the relict repulsive cosmological constant indicated by recent cosmological observations $\Lambda_0 \sim 0.65\Lambda_{\mathrm{crit(0)}} \sim 1.1\times10^{-56}\mathrm{cm}^{-2}$, (b) the primordial effective cosmological constant $\Lambda_{\mathrm{ew}} \sim 0.028\,\mathrm{cm}^{-2}$, and (c) the other possible primordial effective cosmological constant $\Lambda_{\mathrm{qc}} \sim 2.8\times10^{-10}\,\mathrm{cm}^{-2}$.

y	Λ_0		Λ_{ew}		Λ_{qc}	
	M $[M_\odot]$	$r_{\mathrm{mb(o)}}$ [kpc]	M [g]	$r_{\mathrm{mb(o)}}$ [cm]	M [g]	$r_{\mathrm{mb(o)}}$ [cm]
1×10^{-30}	1.1×10^{8}	56	1.4×10^{14}	0.00011	1.4×10^{18}	1.1
1×10^{-29}	3.5×10^{8}	82	4.4×10^{14}	0.00016	4.4×10^{18}	1.6
1×10^{-28}	1.1×10^{9}	130	1.4×10^{15}	0.00024	1.4×10^{19}	2.4
1×10^{-27}	3.5×10^{9}	170	4.4×10^{15}	0.00034	4.4×10^{19}	3.4
1×10^{-26}	1.1×10^{10}	250	1.4×10^{16}	0.00048	1.4×10^{20}	4.8
1×10^{-25}	3.5×10^{10}	360	4.4×10^{16}	0.0007	4.4×10^{20}	7.0
1×10^{-24}	1.1×10^{11}	530	1.4×10^{17}	0.001	1.4×10^{21}	10
1×10^{-23}	3.5×10^{11}	780	4.4×10^{17}	0.0015	4.4×10^{21}	15
1×10^{-22}	1.1×10^{12}	1100	1.4×10^{18}	0.0022	1.4×10^{22}	22
1×10^{-21}	3.5×10^{12}	1700	4.4×10^{18}	0.0032	4.4×10^{22}	32
1×10^{-20}	1.1×10^{13}	2500	1.4×10^{19}	0.0048	1.4×10^{23}	48
1×10^{-19}	3.5×10^{13}	3600	4.4×10^{19}	0.007	4.4×10^{23}	70
1×10^{-18}	1.1×10^{14}	5300	1.4×10^{20}	0.01	1.4×10^{24}	100
1×10^{-17}	3.5×10^{14}	7800	4.4×10^{20}	0.015	4.4×10^{24}	150
1×10^{-16}	1.1×10^{15}	11000	1.4×10^{21}	0.022	1.4×10^{25}	220
1×10^{-15}	3.5×10^{15}	17000	4.4×10^{21}	0.032	4.4×10^{25}	320
1×10^{-14}	1.1×10^{16}	25000	1.4×10^{22}	0.048	1.4×10^{26}	480
1×10^{-13}	3.5×10^{16}	36000	4.4×10^{22}	0.07	4.4×10^{26}	700
1×10^{-12}	1.1×10^{17}	53000	1.4×10^{23}	0.1	1.4×10^{27}	1000
1×10^{-11}	3.5×10^{17}	78000	4.4×10^{23}	0.15	4.4×10^{27}	1500
1×10^{-10}	1.1×10^{18}	110000	1.4×10^{24}	0.22	1.4×10^{28}	2200
1×10^{-9}	3.5×10^{18}	170000	4.4×10^{24}	0.32	4.4×10^{28}	3200
1×10^{-8}	1.1×10^{19}	240000	1.4×10^{25}	0.47	1.4×10^{29}	4700
1×10^{-7}	3.5×10^{19}	350000	4.4×10^{25}	0.68	4.4×10^{29}	6800
1×10^{-6}	1.1×10^{20}	500000	1.4×10^{26}	0.97	1.4×10^{30}	9700
5×10^{-6}	2.5×10^{20}	630000	3.1×10^{26}	1.2	3.1×10^{30}	12000
8.5×10^{-6}	3.2×10^{20}	670000	4×10^{26}	1.3	4×10^{30}	13000
0.00001	3.5×10^{20}	690000	4.4×10^{26}	1.3	4.4×10^{30}	13000
0.00002	5×10^{20}	740000	6.2×10^{26}	1.4	6.2×10^{30}	14000
0.0001	1.1×10^{21}	810000	1.4×10^{27}	1.6	1.4×10^{31}	16000
0.0002	1.6×10^{21}	740000	2×10^{27}	1.4	2×10^{31}	14000
0.00024	1.7×10^{21}	620000	2.1×10^{27}	1.2	2.1×10^{31}	12000

because the largest observed jets extend to distances $\sim 200\,\mathrm{kpc}$ (Blandford 1990), exceeding dimensions of the "seed" galaxy (comparable to the static radius).

It is well known (Carroll & Ostlie 1996) that dimensions of large galaxies, of both spiral and elliptical type, are in the interval 50–100 kpc, while the extremely large elliptical galaxies of cD type extend up to 1000 kpc. Thus, we can conclude that toroidal disks around a central hole of mass $M \sim 10^9\,M_\odot$ have sizes comparable with the large galaxies and can be related to size-limits on these galaxies. On the other hand, such disks are well inside the cD elliptical galaxies; in order to obtain an accretion disk of dimension $\sim 1000\,\mathrm{kpc}$, mass parameter of the central black hole have to be $\sim 10^{12}\,M_\odot$.

Of course, if the mass of a protogalactic disk related to a quasar is higher than the mass of the central black hole, the self-gravitational effects of the disk itself have to be taken into consideration. Nevertheless, we can expect that even in the situation like this the repulsive cosmological constant keeps the presence of the outer cusp enabling outflows of matter from the disk. On the other hand, the collimation effect on jets could be efficient even for small toroidal disks, with outer edge located deeply under the static radius. In such disks the self-gravitational effects could usually be neglected.

In the case of accretion onto primordial black holes in the very early universe, with assumed high values of repulsive cosmological constant, we can expect even stronger effects. Considering the electroweak phase transition at $T_{\mathrm{ew}} \sim 100\,\mathrm{GeV}$, we obtain an estimate of the primordial effective cosmological constant

$$\Lambda_{\mathrm{ew}} \sim 0.028\,\mathrm{cm}^{-2}. \tag{49}$$

Considering the quark confinement at $T_{\mathrm{qc}} \sim 1\,\mathrm{GeV}$, we obtain an estimate of the primordial cosmological constant

$$\Lambda_{\mathrm{qc}} \sim 2.8\times10^{-10}\,\mathrm{cm}^{-2}. \tag{50}$$

It follows from the Table 4 that the accretion onto primordial black holes of mass $M > M_{\rm ew} \sim 2 \times 10^{27}$ g, and $M > M_{\rm qc} \sim 2 \times 10^{31}$ g, respectively, is then forbidden in the disk regime because no equilibrium configurations of perfect fluid are allowed in the corresponding Schwarzschild–de Sitter backgrounds. Of course, the accretion can be realized in quasispherical regime in these spacetimes, however, its character represents an open problem.

Acknowledgements. This work has been supported by the GAČR Grant No.202/99/0261, by the Committee for Collaboration of Czech Republic with CERN and by the Bergen Computational Physics Laboratory project, an EU Research Infrastructure at the University of Bergen, Norway, supported by the European Community – Access to Research Infrastructure Action of the Improving Human Potential Programme. Two of authors (Z. S. and S. H.) would like to acknowledge the perfect hospitality and excellent working conditions at the CERN's Theory Division and the Institute of Physics of the University of Bergen.

References

Abramowicz M.A., 1974, Acta Astron. 24, 45
Abramowicz M.A., Percival M.J., 1997, Class. Quantum Gravit. 14, 2003
Abramowicz M.A., Jaroszyński M., Sikora M., 1978, A&A 63, 221
Abramowicz M.A., Calvani M., Nobili L., 1980, ApJ 242, 772
Blandford R.D., 1987, In: Hawking S.W., Israel W. (eds.) Three hundred years of gravitation. Cambridge University Press, Cambridge, p. 277
Blandford R.D., 1990, In: Courvoisier T. J.-L., Mayor M. (eds.) Active Galactic Nuclei. Saas–Fee Advanced Course 20, Lecture Notes 1990, Swiss Society for Astrophysics and Astronomy, Springer Verlag, Berlin, p. 161
Boyer R.H., 1965, Proc. Cambridge Phil. Soc. 61, 527
Carroll B.W., Ostlie D.A., 1996, An Introduction to Modern Astrophysics. Addison-Wesley Publishing Co., Inc., Reading, Massachusetts, ISBN 0-201-54730-9
Fishbone L.G., 1977, ApJ 205, 323
Fishbone L.G., Moncrief V., 1976, ApJ 207, 962
Jaroszyński M., Abramowicz M.A., Paczyński B., 1980, Acta Astron. 30, 1
Kolb E.W., Turner M.S., 1990, The Early Universe. The Advanced Book Program, Addison-Wesley Publishing Co., Inc., Redwood City, California, ISBN 0-201-11603-0
Kozlowski M., Jaroszyński M., Abramowicz M.A., 1978, A&A 63, 209
Krauss L.M., 1998, ApJ 501, 461
Krauss L.M., Turner M.S., 1995, Gen. Relativ. Gravit. 27, 1137
Lynden-Bell D., 1969, Nat 223, 690
Novikov I.D., Thorne K.S., 1973, In: De Witt C., De Witt B.S. (eds.) Black Holes. Gordon and Breach, New York, p. 343
Ostriker J.P., Steinhardt P.J., 1995, Nat 377, 600
Paczyński B., Wiita P., 1980, A&A 88, 23
Seguin F.H., 1975, ApJ 197, 745
Stoeger W.R., 1976, A&A 53, 267
Stuchlík Z., Hledík S., 1999, Phys. Rev. D 60, 044006